Planetary and Space Science 75 (2013) 11–16

Contents lists available at SciVerse ScienceDirect

Planetary and Space Science

journal homepage: www.elsevier.com/locate/pss

Dust–plasma interaction through magnetosphere–ionosphere coupling in Saturn's plasma disk

Shotaro Sakai [a,*], Shigeto Watanabe [a], Michiko W. Morooka [b], Madeleine K.G. Holmberg [c,d], Jan-Erik Wahlund [c,d], Donald A. Gurnett [e], William S. Kurth [e]

[a] Department of Cosmosciences, Hokkaido University, Kita 10, Nishi 8, Kita-ku, Sapporo 060-0810, Japan
[b] Planetary Plasma and Atmospheric Research Center, Graduate School of Science, Tohoku University, 6-3 Aramaki-Aza-Aoba, Sendai 980-8578, Japan
[c] Swedish Institute of Space Physics, Box 537, SE 751 21 Uppsala, Sweden
[d] Department of Physics and Astronomy, Uppsala University, Box 516, SE 751 20 Uppsala, Sweden
[e] Department of Physics and Astronomy, University of Iowa, Iowa City, IA 522 42, United States

ARTICLE INFO

Article history:
Received 25 April 2012
Received in revised form
5 September 2012
Accepted 7 November 2012
Available online 15 November 2012

Keywords:
Saturn
Dust–plasma interaction
Dusty plasma
Magnetosphere–ionosphere coupling
Co-rotation lag

ABSTRACT

The ion bulk speeds in the equatorial region of Saturn's inner magnetosphere, according to data from the Langmuir Probe (LP) on board the Cassini spacecraft, are about 60% of the ideal co-rotation speed; the ion speeds are between the co-rotation and Keplerian speeds (Holmberg et al., Ion densities and velocities in the inner plasma torus of Saturn, Planetary and Space Science). These findings suggest that sub-micrometer negatively charged E ring dust contributes to the plasma dynamics in the plasma disk.

We calculated the ion speeds by using a multi-species fluid model, taking into account dust interactions to investigate the effects of ion–dust coulomb collision, mass loading, as well as taking into account magnetosphere–ionosphere coupling to investigate the effect of the magnetospheric electric field. The results show that the ion speeds can be significantly reduced by the electric fields generated by the collisions between ions and dusts when the dust density is high and the thickness of dust distribution is large. We also show that the ion speeds from our model are consistent with the LP observations when the maximum density of dust is larger than $\sim 10^5\ m^{-3}$.

© 2012 Elsevier Ltd. All rights reserved.

1. Introduction

Plasma in Saturn's magnetosphere is co-rotating due to the rapid rotation of the planet (e.g., Blanc et al., 2005). However, the magnetosphere can be slowed from the co-rotation speed due to, for instance, mass loadings (e.g., Hill, 1979; Saur et al., 2004). Past observations using the particle detectors on Voyager and Cassini showed that around 5 R_S (1 R_S=60,268 km), the plasma speeds are almost the ideal co-rotation speed and gradually decrease to 70–80% of that speed at 7 R_S (Bridge et al., 1981, 1982; Richardson, 1986, 1998; Wilson et al., 2008, 2009).

Observations using the Langmuir Probe (LP) on board the Cassini spacecraft showed that part of the ion bulk speeds are close to the Keplerian speed in Saturn's E ring (Wahlund et al., 2009), which is consistent with the presence of small (micro- and nano-sized) dust particles. These dust particles are negatively charged inside 7 R_S and are expected to contribute to the electrodynamics of the plasma disk structure (Horányi et al., 2004; Kempf et al., 2008). Near Enceladus, which is a major source of the E ring dust, the electron density is significantly less than the ion density and the ion speeds are near Keplerian within a large region (Morooka et al., 2011). The ion beam spectrometer of the Cassini Plasma Spectrometer (CAPS/IBM) on board Cassini also observed that the ions slow to 50–90% of the ideal co-rotation speed (Thomsen et al., 2010).

In the latest observations by the LP, data collected from February 2005 to June 2010 (Rev 003–133) were used Holmberg et al. (in press). They showed the ion speeds are much less than the ideal co-rotation speed in the inner magnetosphere. The speeds were 50–70% of the ideal co-rotation speed. As suggested by Wahlund et al. (2009), the charged dust particles in the E ring were related to the lower ion speeds. Some ion speeds were also smaller than the Keplerian speed around 4 R_S. This could happen if the ions were related to Enceladus (Shafiq et al., 2011). The ion speeds found here were less than those reported by Wilson et al. (2008) and Thomsen et al. (2010) from the CAPS data. Wilson et al. (2008) found ion speeds around 80% of the ideal co-rotation speed between 5 R_S and 10 R_S, and Thomsen et al. (2010) found ion speeds of 50–90% of the ideal co-rotation speed. This could be owing to the difference in the measured particle energy range in measurement methods between the LP and the CAPS/IBS.

* Corresponding Author. Tel.: +81117064689.
E-mail address: shotaro@ep.sci.hokudai.ac (S. Sakai).

0032-0633/$ - see front matter © 2012 Elsevier Ltd. All rights reserved.
http://dx.doi.org/10.1016/j.pss.2012.11.003

In this paper, we report the results of modeling ion speeds in the inner magnetosphere by using a multi-species fluid model taking into account the dust–plasma interaction and mass loadings.

2. Model

2.1. A multi-species fluid model

We calculate the ion and dust velocities by using a multi-species fluid model (i.e., protons, water group ions, charged dusts and electrons) to investigate the effect of dust on ion speed.

$$\frac{\partial \rho_k}{\partial t}+\nabla\cdot(\rho_k\mathbf{v}_k)=S_k-L_k, \tag{1}$$

$$\frac{\partial(\rho_k\mathbf{v}_k)}{\partial t}+\nabla\cdot(\rho_k\mathbf{v}_k\mathbf{v}_k)=n_kq_k(\mathbf{E}+\mathbf{v}_k\times\mathbf{B})-\nabla p_k-\rho_k\mathbf{g}-\sum_l\rho_k\nu_{kl}(\mathbf{v}_k-\mathbf{v}_l)+\sum_l S_{k,l}\mathbf{v}_l-L_k\mathbf{v}_k \tag{2}$$

Here, subscript k indicates proton (p), water group ion (w), dust (d), or electron (e); ρ_k is m_kn_k; $\mathbf{v}_k$ is velocity; m_k is mass; q is charge quantity (i.e., e is the charge quantity of ions and electrons, and q_d is that of dust); $\mathbf{E}$ is the electrical field vector; $\mathbf{B}$ is the magnetic field vector; ν_{kl} is the general collision frequency considering collisions among the ions, dust, electrons, and neutral gases; where n_k is the number density. The ion production rate is given by

$$S_{k,l}=m_s\kappa n_sn_l+m_kn_l\int_0^\infty\sigma_kFd\lambda, \tag{3}$$

where κ is the reaction rate of the production, σ_k is the scattering cross section, F is the density of photons, and λ is wavelength. The total ionization frequency of water group ions is

$$\int_0^\infty\sigma_iFd\lambda=1.184\times10^{-8}\ (\mathrm{s}^{-1}), \tag{4}$$

which is converted to a Saturn value based on an Earth value (Schunk and Nagy, 2009). We set the mass loading of dust to zero since it is negligibly small. The ion loss term is given by

$$L_{k,l}=m_k\alpha n_kn_l, \tag{5}$$

where α is the reaction rate of the loss. From Eqs. (1) and (2), we finally can obtain

$$\rho_k\frac{\partial\mathbf{v}_k}{\partial t}+\rho_k(\mathbf{v}_k\cdot\nabla)\mathbf{v}_k=n_kq_k(\mathbf{E}+\mathbf{v}_k\times\mathbf{B})-\nabla p_k-\rho_k\mathbf{g}-\sum_l\rho_k\nu_{kl}(\mathbf{v}_k-\mathbf{v}_l)-\sum_l S_{k,l}(\mathbf{v}_k-\mathbf{v}_l) \tag{6}$$

We use Eq. (6) for the ion speed calculations in the Saturn's inner magnetosphere. The ions generated by the charge exchange are H^+, H_2O^+, H_3O^+, OH^+, and O^+. The chemical equations and the reaction rates are listed in Table 1.

Collision frequencies are given by

$$\nu_{id}=n_d\left\{4\pi\left[\frac{q_de}{4\pi\varepsilon_0m_i\left(|\mathbf{v}_i-\mathbf{v}_d|^2+\nu_{thi}^2\right)}\right]^2+\pi r_d^2\right\}\sqrt{|\mathbf{v}_i-\mathbf{v}_d|^2+\nu_{thi}^2}, \tag{7}$$

$$\nu_{ed}=\frac{2\sqrt{2\pi}}{3}n_d\nu_{the}r_d^2\left(\frac{e\phi_s}{k_BT_e}\right)^2\ln\left(\frac{2k_BT_e}{e\phi_sr_d}\lambda_D\right), \tag{8}$$

$$\nu_{ei}=54.5\times10^{-6}\frac{n_i}{T_i^{3/2}}, \tag{9}$$

$$\nu_{in}=\left(2.6\times10^{-15}\right)(n_n+n_i)A^{-1/2}, \tag{10}$$

$$\nu_{en}=\left(5.4\times10^{-10}\right)n_nT_e^{-1/2}, \tag{11}$$

$$\nu_{dn}=n_n\pi r_n^2\sqrt{|\mathbf{v}_d-\mathbf{v}_n|^2+\nu_{thd}^2}, \tag{12}$$

$$\nu_{wp}=1.27\frac{\mu}{M_w}\frac{n_p}{T_i^{3/2}} \tag{13}$$

$$\nu_{kl}=\frac{m_ln_l}{m_kn_k}\nu_{lk}, \tag{14}$$

where subscript i identifies the component of protons and water group ions, respectively, r_d is the dust radius, ϕ_s is the dust surface potential, ν_{thi} is the ion thermal velocity, ν_{the} is the electron thermal velocity, ν_{thd} is the dust thermal velocity, n_n is the neutral number density, M_w is the mass of the water group ion in atomic mass units, μ is the reduced mass between the proton and the water group ion in atomic mass units, and n_p is the proton number density. We used the model of ν_{ed} introduced by Khrapak et al. (2004). The Debye length of a dusty plasma is given by

$$\lambda_D=\sqrt{\frac{\varepsilon_0k_BT_e}{n_ee^2}}, \tag{15}$$

where λ_D is the electron Debye length.

We considered magnetospheric electric fields through the magnetosphere–ionosphere coupling. The electric field $\mathbf{E}$ is given by

$$\Sigma_i(\mathbf{E}_{cor}-\mathbf{E})=\mathbf{j}D, \tag{16}$$

where Σ_i is the ionospheric Pedersen conductivity, $\mathbf{E}_{cor}$ is the co-rotational electric field, and D is the thickness of the dust distribution in z-direction (Fig. 1). $\mathbf{j}$ is the magnetospheric Pedersen current density given by

$$\mathbf{j}=en_p\mathbf{v}_p+en_w\mathbf{v}_w-en_e\mathbf{v}_e-q_dn_d\mathbf{v}_d. \tag{17}$$

2.2. Parameters

Density distributions of electrons, protons, dust particles, and neutral particles are shown in Fig. 2. The densities depend on the distance from Saturn (R_S). Black solid lines indicate electron density, black dashed lines indicate ion density, black dashed–dotted lines indicate proton density, grey solid lines indicate dust density, and grey dashed lines indicate neutral density in each panel. We used density distributions of electrons that are increasing with distance from Saturn inside 5 R_S and are decreasing with distance from Saturn outside 5 R_S (Persoon et al., 2005, 2009). The maximum densities for electrons are $4\times10^7\ \mathrm{m}^{-3}$ (Persoon et al., 2005, 2009) at about 4 R_S. On the other hand, density distributions of neutral gases are decreasing with distance from Saturn. The maximum densities for neutrals are $6.5\times10^8\ \mathrm{m}^{-3}$ (Smith et al., 2010) at 2 R_S. The dust density, n_d, is free parameters. We calculate the ion speeds in two cases: (a) $n_d=1.2\times10^4\ \mathrm{m}^{-3}$, (b) $3.2\times10^4\ \mathrm{m}^{-3}$ at 2 R_S. The number density of water group ion is derived from charge neutrality:

$$n_w=n_e+\frac{q_d}{e}n_d-n_p \tag{18}$$

We use 20% as the ratio of n_p to n_W. The thickness of the dust distribution, D, is used in three cases: $D=1$, 2, and 3 R_S (Table 2). The radius of dust is $r_d=10^{-7}$ m. The Cosmic Dust Analyzer (CDA) can investigate the dust particles size of about 0.8 mm (Kempf et al., 2008). The smaller size and high-density dust was more important in electrodynamics than micro size and low-density dust. Therefore, we used 0.1 μm as the grain radius.

Table 1
Ion chemical reactions and rates used in this study.

Reactions	Rates [$m^3\ s^{-1}$]	References
$H^+ + H_2O \rightarrow H + H_2O^+$	2.60×10^{-15}	Burger et al. (2007); Lindsay et al. (1997)
$O^+ + H_2O \rightarrow O + H_2O^+$	2.13×10^{15}	Burger et al. (2007); Dressler et al. (2006)
$H_2O^+ + H_2O \rightarrow H_2O + H_2O^+$	5.54×10^{-16}	Burger et al. (2007); Lishawa et al. (1990)
$H_2O^+ + H_2O \rightarrow OH + H_3O^+$	3.97×10^{-16}	Burger et al. (2007); Lishawa et al. (1990)
$OH^+ + H_2O \rightarrow OH + H_2O^+$	5.54×10^{-16}	Burger et al. (2007); Itikawa and Mason (2005)
$H_2O + e \rightarrow H_2O^+ + 2e$		Burger et al. (2007); Itikawa and Mason (2005)
$H_2O + e \rightarrow OH^+ + H + 2e$	10^{-18} (total)	Burger et al. (2007); Itikawa and Mason (2005)
$H_2O + e \rightarrow O^+ + H_2 + 2e$		Burger et al. (2007); Itikawa and Mason (2005)
$H_2O + e \rightarrow H^+ + OH + 2e$	10^{-22}	Burger et al. (2007); Itikawa and Mason (2005)

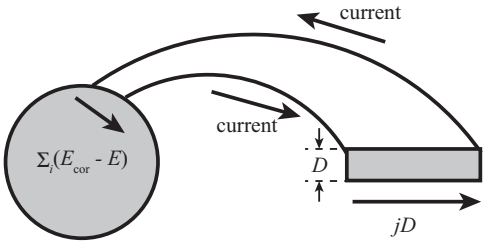

Fig. 1. A cartoon of an electric circuit connecting between magnetosphere and ionosphere.

The charged quantity of dust is

$$q_d = \beta 4\pi\varepsilon_0 r_d \phi_s \ [C]. \tag{19}$$

where β is a function of ion mass and is about 3.66 for water group ions. Each thermal energy is 2 eV since newly created ions from, e.g., photo-ionization would initially have a small energy (Wahlund et al., 2009; Gustafsson and Wahlund, 2010), the dust surface potential is -2 V (Wahlund et al., 2005). The equilibrium spacecraft potential with respect to plasma estimated using the LP includes components from cold and hot electrons as well as effects from secondary and photoelectron emissions and is considered to be a reasonable proxy for grain surface potential for grains of all sizes above about 50 nm (Shafiq et al., 2011). Moreover, the LP observations (Wahlund et al., 2005) during Saturn orbit insertion (SOI) inbound pass is consistent with the electrostatic equilibrium potential of the dust grains in Saturn's inner magentosphere measured by the CDA (Kempf et al., 2006). The mass of water group ions and neutral gases are 18 m_p. The mass of dust is

$$m_d = \frac{4\pi\rho r_d^3}{3} \ \text{(kg)} \tag{20}$$

since the bulk density of dust made from water ice is given by $\rho = 10^3$ kg m^{-3}, and the ionospheric conductivity Σ_i is 1 S (Cowley and Bunce, 2003). Cowley and Bunce (2003) indicated that the conductivity was of the order of $\sim$1 S or less in the middle latitude ionosphere. We used 1 S as the Pedersen conductivity.

2.3. Boundary condition

We calculate the steady-state solutions of proton, water groups ion and dust speeds. A grid size is 0.1 R_S from 2 to 10 R_S in radial direction. Initial speeds of each ion are the co-rotation speed and initial speed of dust is the Keplerian speed. Speeds at 2 R_S of each ion are fixed to the co-rotation speed and gradients of each ion speed at outer boundary are zero. On the other hand, dust speed at 2 R_S is the Keplerian speed and gradient of dust speed at outer boundary is zero. We assume that the electron has the co-rotation speeds from 2 to 10 R_S.

3. Results

The observations from LP reveal that ion speeds are much smaller than the co-rotation speed and a large amount of cold ions interact with negatively charged dust particles (Holmberg et al., in press).

To explain these results, we investigate the effect of coulomb collisions between the ions and dust particles, the mass loading, the charge exchange and the magnetospheric electric field. The parameters are the density and thickness of the dust distribution. Fig. 3 shows the relationship of distance from Saturn with ion speed, current density, generated magnetospheric electric field and frequency. The red line indicates the ideal co-rotation speed, and the blue line indicates the Keplerian speed; furthermore, the orange, yellow and green lines indicate the ion speed when the thickness of dust distribution, D, is 1 R_S, 2 R_S and 3 R_S, respectively. The second panels show the current density; the colors denote the same meaning as in the top panels. The third panels show the electric field generated by the difference of motions among ions, electrons and dusts; the colors denote the same meaning as in the top panels. The bottom panels show the frequency profile. The red line in the bottom panels indicates the ion cyclotron frequency and the other line indicates the ion–dust collision frequency, ν_{wd}. Fig. 3a is the case of $n_{d,r=2R_S} = 1.2 \times 10^4$ m^{-3} (Case 1, 3 and 5 in Table 2) and Fig. 3b is the case of $n_{d,r=2R_S} = 3.2 \times 10^4$ m^{-3} (Case 2, 4 and 6 in Table 2).

Ion speeds are the ideal co-rotation speed within about 3 R_S in all cases (Fig. 3). However, the ion speeds start to decrease from the ideal co-rotation speed around 3 R_S. The ion speeds are 50–90% of the ideal co-rotation speed less than about 5 R_S (top panel in Fig. 3). On the other hand, the ion speeds are close to the ideal co-rotation speed larger than about 5 R_S since the dust density is less than that it the inner region (Fig. 3). The generated electric field is 10^{-4} to 10^{-2} V m^{-1} within about 6 R_S. However, it is about 10^{-5}–10^{-4} V m^{-1} outside of 5 R_S (third panel in Fig. 3). The magnetospheric electric field is smaller than the co-rotational electric field when current flows in the magnetosphere. Therefore, the ion speeds decrease from the ideal co-rotation speed. However, the local current density is not relevant to the thickness of dust distribution, D (middle panel in Fig. 3). The magnetospheric electric field is determined by the magnetosphere–ionosphere coupling. A current flowing the ionosphere is equivalent to the magnetospheric current from the conservation law of current. The thickness of dust distribution is important parameter for a total current flowing the magnetosphere since the total current depends on D. The generated magnetospheric electric field is smaller when D is large. The green lines in Fig. 3 are about 80% of the orange lines around 5 R_S (top panel in Fig. 3). For the generated magetospheric electric field, the green line is larger than the orange line (third panel in Fig. 3). Therefore, the ion speeds also depend on D and they are smaller when D is large. The generated magnetospheric electric field also depends on each

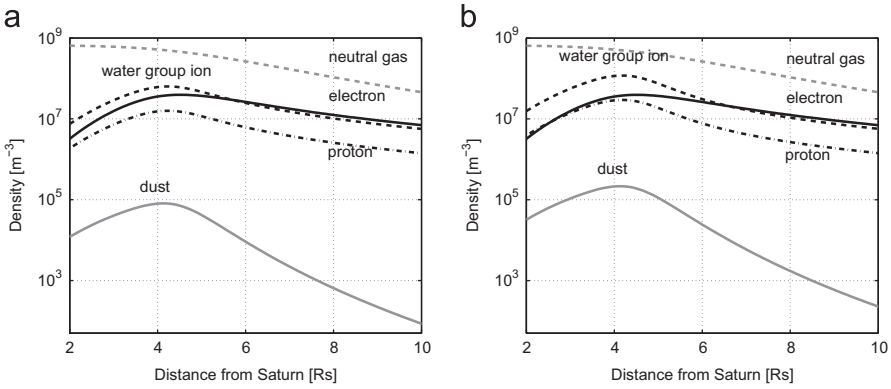

Fig. 2. Density profiles. Black solid line indicates electron density, black dashed line indicates water group ion density, black dashed-dotted line indicates proton density, and grey solid line indicates dust density, and grey dashed line indicates neutral density. (a) $n_{d,r=2R_S}=1.2\times10^4$ m^{-3}; (b) $n_{d,r=2R_S}=3.2\times10^4$ m^{-3}.

Table 2
Modeling parameters.

	Dust density at 2 R_S (m^{-3})	Thickness of dust distribution (R_S)
Case 1	1.2×10^4, panel (a) in Fig. 2	1 R_S
Case 2	3.2×10^4, panel (b) in Fig. 2	
Case 3	1.2×10^4, panel (a) in Fig. 2	2 R_S
Case 4	3.2×10^4, panel (b) in Fig. 2	
Case 5	1.2×10^4, panel (a) in Fig. 2	3 R_S
Case 6	3.2×10^4, panel (b) in Fig. 2	

density since the magnetospheric total current is determined by each density, especially ion density. The ion density increase when dust density increase (see Eq. (17)). It means that the variation of the dust density is important for the electric field. The ion speeds in Fig. 3b (corresponding to Cases 2, 4 and 6) are less than those in Fig. 3a (Cases 1, 3 and 5). Therefore, the ion speeds are smaller when the dust density is larger. On the other hand, the collisions between ions and dust particles do not have a direct effect on ion speed because v_{wd} is much smaller than the ion cyclotron frequency (red line of bottom panel in Fig. 3).

From these results, the ions interact with the dusts through magnetosphere–ionosphere coupling when the thickness of the dust distribution and the dust density is large. The ions are slowing from the ideal co-rotation speed.

4. Discussion

We calculated the ion speeds by using a multi-species fluid model. Our calculations show that the ion speed becomes smaller than the ideal co-rotation speed as a result of coulomb collisions with dust and mass loading, and the magnetosphere–ionosphere coupling is considerably important through the ion–dust collision in Saturn's inner magnetosphere. Ion observations by the LP onboard the Cassini indicate that ion speed increases as the distance from Saturn increases (Holmberg et al., in press). The ion speeds in the plasma disk are 50–70% of co-rotation speed within 7 R_S.

Our modeling results are consistent with LP observations when the dust density is large (Fig. 4b). Our results are also consistent with observations even if the dust density is small if the thickness of dust distribution, D, is large (green line in Fig. 4a). The ion speeds strongly depend on the magnetospheric electric field. The magnetospheric electric field is governed by the inner magnetospheric total Pedersen current, and the Pedersen current is generated by the collisions and the mass loading. The Pedersen current flows along the magnetic field line and weaken the dynamo electric field in Saturn's ionosphere. Accordingly, the magnetospheric electric field is smaller than the co-rotational electric field and the ion speeds are less than the ideal co-rotation speed. The magnitude of the Pedersen current is dependent on each density and D. Higher Pedersen current flows in the inner magnetosphere when each density or D is large. Since more density is needed when D is small, we suggest that the maximum of dust density is larger than $\sim10^5$ m^{-3} in Saturn's inner magnetosphere (Fig. 4).

Morooka et al. (2011) reported that the ion speeds are nearly the Keplerian speed and that the densities of ions and dusts are large in the vicinity of Enceladus. The ion and dust densities are much larger in this region due to the Enceladus plume. Under this condition, the total current due to ion–dust collision is much larger than that in other regions since the current is proportional to the densities. We note that the ion speed approaches the Keplerian speed when the dust density is larger than about 10^6 m^{-3}.

Wahlund et al. (2009) suggested the existence of two ion populations: one co-rotating with the planetary magnetosphere and another moving at near Keplerian speed around Saturn. Hot ions (ca. 10–50 eV) are co-rotating without being trapped by dust, and cold ions (a few electron volts) are slowed from the co-rotation speed by the dust drag. From the LP observations of particles of a few electron volts, we obtained much lower ion speeds, including values less than 50% of the ideal co-rotation speed. On the other hand, from CAPS observations of particles of a few hundred electron volts, ion speeds are 50–80% of the ideal co-rotation (Wilson et al., 2008, 2009; Thomsen et al., 2010). Taken together, the results from CAPS and LP observations show that two ion populations exist in Saturn's inner magnetosphere, as suggested by Wahlund et al. (2009).

In other models, co-rotational lag has an effect outside the inner magnetosphere (Hill, 1979; Saur et al., 2004). Saur et al. (2004) accounted for radial mass transport and magnetospheric conductance in their model. Their results were ion speeds less than the ideal co-rotation beyond 5 R_S. Our results show that the ion speeds are the ideal co-rotation speed within 3 R_S, which is consistent with the results of Saur et al. (2004) within 3 R_S.

Kurth et al. (2006) reported a vertical distribution of dust near Enceladus' orbit using the RPWS. The thickness of dust distribution is about 15,000 km ($\sim$0.25 R_S). On the other hand, a ratio of an electron density to an ion density (n_e/n_i) in Morooka et al. (2011) is less than one between -80 R_E and 50 R_E (1 R_E=251.8 km is the radius of Enceladus), which is corresponding to about 0.6 R_S. However, we estimated the thickness of dust distributions at from 1 to 3 R_S since the density profile of the vertical direction higher than 50 R_E and lower than 80 R_E is not reported and n_e/n_i is not one

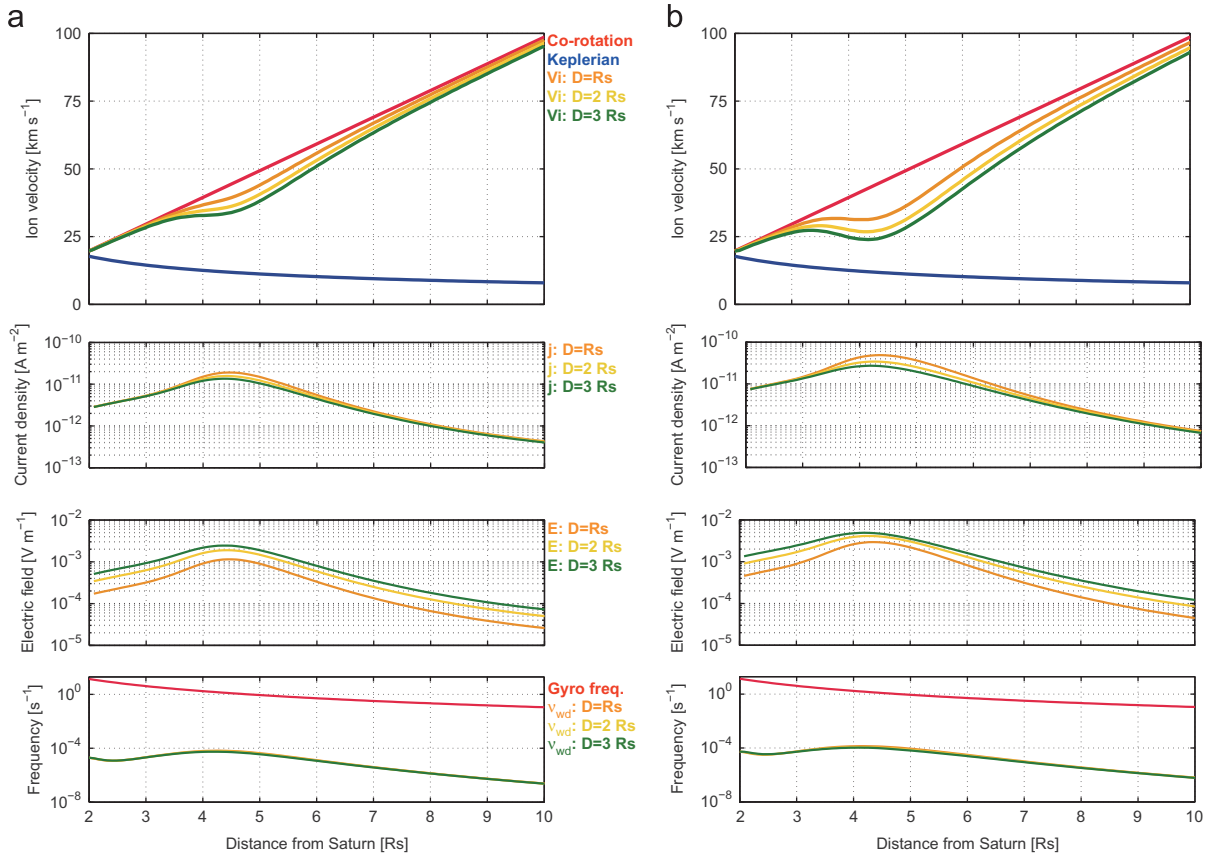

Fig. 3. Modeling results. (a) $n_{d,r=2R_S} = 1.2 \times 10^4$ m^{-3}; (b) $n_{d,r=2R_S} = 3.2 \times 10^4$ m^{-3}. (Top) Ion velocity profile. Red line indicates the ideal co-rotation speed, and blue line indicates the Keplerian speed. Orange, yellow and green lines indicate ion velocities calculated when the thickness of dust distribution, D, is 1 R_S, 2 R_S and 3 R_S, respectively. (Second) Total current density profile. Orange, yellow and green lines indicate current density calculated when the thickness of dust distribution is 1 R_S, 2 R_S and 3 R_S, respectively. (Third) Electric field generated by the difference of motion among ions, electrons and dusts. Orange, yellow and green lines indicate a magnetospheric electric field calculated when the thickness of dust distribution is 1 R_S, 2 R_S and 3 R_S, respectively. (Bottom) Ion–dust collision frequency profile. Red line indicates ion cyclotron frequency for water group. Orange, yellow and green lines indicate ion–dust collision frequencies calculated when the thickness of dust distribution is 1 R_S, 2 R_S and 3 R_S, respectively.

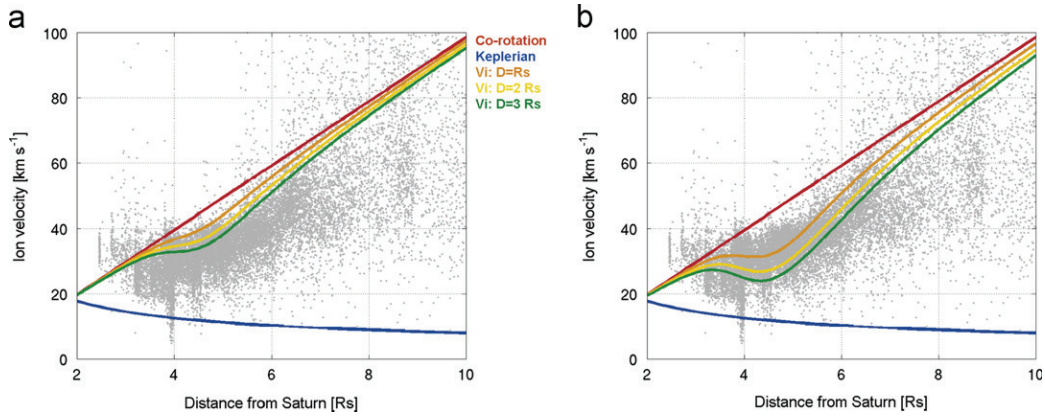

Fig. 4. Comparisons between modeling results and RPWS/LP observations. (a) $n_{d,r=2R_S} = 1.2 \times 10^4$ m^{-3}; (b) $n_{d,r=2R_S} = 3.2 \times 10^4$ m^{-3}. Ion velocities are superposed on the LP observations from Holmberg et al. in press. Grey dots are observation points, red line indicates the ideal co-rotation speed, and blue line indicates the Keplerian speed. Orange, yellow and green lines indicate ion velocities calculated when the thickness of dust distribution, D, is 1 R_S, 2 R_S and 3 R_S, respectively.

at -80 R_E and 50 R_E. If the thickness of dust distribution is 1 R_S, the maximum of dust density needs at least 10^5 m^{-3}. Moreover, a more accurate treatment of the dust and the ionosphere could affect our results. The reality is a dust distribution with a size, mass and charge. The ionospheric conductivity could also affect the generated magnetospheric electric field. Therefore, we need to consider the dust distribution and the ionospheric conductivity in the next study.

Many observations have found strong planetary rotational modulation of Saturn's magnetospheric plasma despite the nearly parallel alignment of the magnetic dipole and the planetary axis (Gurnett et al., 2007; Kurth et al., 2008). This modulation causes the magnetodisc plasma to wobble with respect to the E ring (Goertz et al., 1981). The interaction between dust and ions in the E ring will be enhanced once each planetary spin axis, showing

the longitude dependence of ion and dust parameters (Fig. 8 in Morooka et al., 2011). Kurth et al. (2008) showed a clear relationship between the Cassini spacecraft potential of the plasma disk and longitude of the Saturn Longitude System. Gurnett et al. (2007) also reported that the plasma and magnetic fields in the Saturn's plasma disk rotate in synchronism with the time-variable modulation period of Saturn's kilometric radio emission. As mentioned above, the longitudinal dependence of parameters, e.g., ion speed and density, may be important in explaining the planetary rotational modulations.

5. Conclusion

We calculated the ion drift speed using a multi-species fluid model (i.e., protons, water group ions, electrons, and charged dusts) in order to examine the effect of dust on ion speed. In agreement with the LP observations, the modeling results showed that the ion speeds are less than the co-rotation speed. The ion speeds are possibly less than the co-rotation speed as a result of the magnetospheric electric field generated through ion–dust collisions.

Dust–plasma interaction occurs through magnetosphere–ionosphere coupling. The inner magnetospheric total current along a magnetic field line weakens the dynamo electric field in Saturn's ionosphere. The ion speeds are Keplerian due to the large total current when the ion and dust densities are large. The dust–plasma interaction is significant when the thickness of the dust distribution is large and/or the density of ions and dusts is high.

Acknowledgement

This work was supported by a research fellowship of the Japan Society for the Promotion of Science (JSPS).

References

Blanc, M.F., Kallenbach, R., Erkaev, N.V., 2005. Solar system magnetospheres. Space Science Review 116, 227–298, http://dx.doi.org/10.1007/s11214-005-1958-y.

Burger, M.H., Sittler Jr., E.C., Johnson, R.E., Smith, H.T., Tucker, O.J., Shematovich, V.I., 2007. Understanding the escape of water from Enceladus. Journal of Geophysical Research 112, A06219, http://dx.doi.org/10.1029/2006JA012086.

Bridge, H.S., Belcher, J.W., Lazarus, A.J., Olbert, S., Sullivan, J.D., Bagenal, F., Gazis, P.R., Hartle, R.E., Ogilvie, K.W., Scudder, J.D., Sittler, E.C., Eviatar, A., Siscoe, G.L., Goertz, C.K., Vasyliunas, V.M., 1981. Plasma observations near Saturn—initial results from Voyager 1. Science 212, 217–224, http://dx.doi.org/10.1126/science.212.4491.217.

Bridge, H.S., Bagenal, F., Belcher, J.W., Lazarus, A.J., McNutt, R.L., Sullivan, J.D., Gazis, P.R., Hartle, R.E., Ogilvie, K.W., Scudder, J.D., Sittler, E.C., Eviatar, A., Siscoe, G.L., Goertz, C.K., Vasyliunas, V.M., 1982. Plasma observations near Saturn—initial results from Voyager 2. Science 215, 563–570, http://dx.doi.org/10.1126/science.215.4532.563.

Cowley, S.W.H., Bunce, E.J., 2003. Corotation-driven magnetosphere–ionosphere coupling currents in Saturn's magnetosphere and their relation to the auroras. Annales Geophysicae 21, 1691–1707, http://dx.doi.org/10.5194/angeo-21-1691-2003.

Dressler, R.A., Bastian, M.J., Levandier, D.J., Murad, E., 2006. Emperical model of the state-state dynamics in near-resonant hyperthermal $X^+ + H_2O$ charge-transfer reactions. International Journal of Mass Spectrometry 159, 245–256.

Goertz, C.K., Thomsen, M.F., Ip, W.–H., 1981. Saturn's radio emissions: rotational modulation. Nature 292, 737–739, http://dx.doi.org/10.1038/292737a0.

Gurnett, D.A., Persoon, A.M., Kurth, W.S., Groene, J.B., Averkamp, T.F., Dougherty, M.K., Southwood, D.J., 2007. The variable rotation period of the inner region of Saturn's plasma disk. Science 316, 442–445, http://dx.doi.org/10.1126/science.1138562.

Gustafsson, G., Wahlund, J.–E., 2010. Electron temperatures in Saturn's plasma disc. Planetary and Space Science 58, 1018–1025, http://dx.doi.org/1016/j.pss.2010.03.007.

Hill, T.W., 1979. Inertial limit on corotation. Journal of Geophysical Research 84, 6554–6558, http://dx.doi.org/10.1029/JA084iA11p06554.

Holmberg, M.K.G., Wahlund, J.–E., Morooka, M.W., Persoon, A.M. Ion densities and velocities in the inner plasma torus of Saturn, Planetary and Space Science, http://dx.doi.org/10.1016/j.pss.2012.09.016, in press.

Horányi, M., Hartquist, T.W., Havnes, O., Mendis, D.A., Morfill, G.E., 2004. Dusty plasma effects in Saturn's magnetosphere. Reviews of Geophysics 42, RG4002, http://dx.doi.org/10.1029/2004RG000151.

Itikawa, Y., Mason, N., 2005. Cross sections for electron collisions with water molecules. Journal of Physical and Chemical Reference Data 34, 1.

Kempf, S., Beckmann, U., Srama, R., Horanyi, M., Auer, S., Grün, E., 2006. The electrostatic potential of E ring particles. Planetary and Space Science 54, 999–1006, http://dx.doi.org/10.1016/j.pss.2006.05.012.

Kempf, S., Beckmann, U., Moragas-Klostermeyer, G., Postberg, F., Srama, R., Economou, T., Schmidt, J., Spahn, F., Grün, E., 2008. The E ring in the vicinity of Enceladus, I. Spatial distribution and properties of the ring particles. Icarus 193, 420–437, http://dx.doi.org/10.1016/j.icarus.2007.06.027.

Khrapak, S.A., Ivlev, A.V., Morfill, G.E., 2004. Momentum transfer in complex plasmas. Physical Review 70, 056405, http://dx.doi.org/10.1103/PhysRevE.70.056405.

Kurth, W.S., Averkamp, T.F., Gurnett, D.A., Wang, Z., 2006. Cassini RPWS observations of dust in Saturn's E ring. Planetary and Space Science 54, 988–998, http://dx.doi.org/10.1016/j.pss.2006.05.011.

Kurth, W.S., Averkamp, T.F., Gurnett, D.A., Groene, J.B., Lecacheux, A., 2008. An update to a Saturnian longitude system based on kilometric radio emissions. Journal of Geophysical Research 113, A05222, http://dx.doi.org/10.1029/2007JA012861.

Lindsay, B.G., Sieglaff, D.R., Smith, K.A., Stebbings, R.F., 1997. Charge transfer of 0.5-, 1.5-, and 5-keV protons with H_2O: absolute differential and integral cross sections. Physical Review A 55, 3945–3946.

Lishawa, C.R., Dressler, R.A., Gardner, J.A., Salter, R.H., Murad, E., 1990. Cross sections and product kinetic energy analysis of H_2O+-H_2O collisions at suprathermal energies. Journal of Chemical Physics 93, 3196–3206.

Morooka, M.W., Wahlund, J.E., Eriksson, A.I., Farrell, W.M., Gurnett, D.A., Kurth, W.S., Persoon, A.M., Shafiq, M., André, M., Holmberg, M.K.G., 2011. Dusty plasma in the vicinity of Enceladus. Journal of Geophysical Research 116, A12221, http://dx.doi.org/10.1029/2011JA017038.

Persoon, A.M., Gurnett, D.A., Kurth, W.S., Hospodarsky, G.B., Groene, J.B., Canu, P., Dougherty, M.K., 2005. Equatorial electron density measurements in Saturn's inner magnetosphere. Geophysical Research Letters 32, L23105, http://dx.doi.org/10.1029/2005GL024294.

Persoon, A.M., Gurnett, D.A., Santolik, O., Kurth, W.S., Faden, J.B., Groene, J.B., Lewis, G.R., Coates, A.J., Wilson, R.J., Tokar, R.L., Wahlund, J.E., Moncuquet, M., 2009. A diffusive equilibrium model for the plasma density in Saturn's magnetosphere. Journal of Geophysical Research 114, A04211, http://dx.doi.org/10.1029/2008JA013912.

Richardson, J.D., 1986. Thermal ions at Saturn: plasma parameters and implications. Journal of Geophysical Research 91, 1381–1389, http://dx.doi.org/10.1029/JA091iA02p01381.

Richardson, J.D., 1998. Thermal plasma and neutral gas in Saturn's magnetosphere. Reviews of Geophysics 36, 501–524, http://dx.doi.org/10.1029/98RG01691.

Saur, J., Mauk, B.H., Kaßner, A., Neubauer, F.M., 2004. A model for the azimuthal plasma velocity in Saturn's magnetosphere. Journal of Geophysical Research 109, A05217, http://dx.doi.org/10.1029/2003JA010207.

Schunk, R.W., Nagy, A.F., 2009. Ionization and energy exchange processes in ionospheres: physics, plasma physics, and chemistry. In: Houghton, J.T., Rycroft, M.J., Dessler, A.J. (Eds.), The Edinburgh Building, Cambridge CB2 8RU. Cambridge University Press, Cambridge, England, United Kingdom, pp. 54–288.

Shafiq, M., Wahlund, J.E., Morooka, M.W., Kurth, W.S., Farrell, W.M., 2011. Characteristics of the dust–plasma interaction near Enceladus' SouthPole. Planetary and Space Science 59, 17–25, http://dx.doi.org/10.1016/j.pss.2010.10.006.

Smith, H.T., Johnson, R.E., Perry, M.E., Mitchell, D.G., McNutt, R.L., Young, D.T., 2010. Enceladus plume variability and the neutral gas densities in Saturn's magnetosphere. Journal of Geophysical Research 115, A10252, http://dx.doi.org/10.1029/2009JA015184.

Thomsen, M.F., Reisenfeld, D.B., Delapp, D.M., Tokar, R.L., Young, D.T., Crary, F.J., Sittler, E.C., McGraw, M.A., Williams, J.D., 2010. Survey of ion plasma parameters in Saturn's magnetosphere. Journal of Geophysical Research 115, A10220, http://dx.doi.org/10.1029/2010JA015267.

Wahlund, J.–E., Boström, R., Gustafsson, G., Gurnett, D.A., Kurth, W.S., Averkamp, T., Hospodarsky, G.B., Persoon, A.M., Canu, P., Pedersen, A., Desch, M.D., Eriksson, A.I., Gill, R., Morooka, M.W., André, M., 2005. The inner magnetosphere of Saturn: Cassini RPWS cold plasma results from the first encounter. Geophysical Research Letters L20, S09, http://dx.doi.org/10.1029/2005GL022699.

Wahlund, J.–E., André, M., Eriksson, A.I.E., Lundberg, M., Morooka, M.W., Shafiq, M., Averkamp, T.F., Gurnett, D.A., Hospodarsky, G.B., Kurth, W.S., Jacobsen, K.S., Pedersen, A., Farrell, W., Ratynskaia, S., Piskunov, N., 2009. Detection of dusty plasma near the E-ring of Saturn. Planetary and Space Science 57, 1795–1806, http://dx.doi.org/10.1016/j.pss.2009.03.011.

Wilson, R.J., Toker, R.L., Henderson, M.G., Hill, T.W., Thomsen, M.F., Pontius Jr., D.H., 2008. Cassini plasma spectrometer thermal ion measurements in Saturn's inner magnetosphere. Journal of Geophysical Research 113, A12218, http://dx.doi.org/10.1029/2008JA013486.

Wilson, R.J., Toker, R.L., Henderson, M.G., 2009. Thermal ion flow in Saturn's inner magnetophere measured by the Cassini plasma spectrometer: a signature of the Enceladus torus? Geophysical Research Letters 36, L23104, http://dx.doi.org/10.1029/2009GL040225.